Title
Probing Complex Chemical Processes at the Molecular Level with Vibrational Spectroscopy and X–ray Tools

Journal
The Journal of Physical Chemistry Letters, 14(41)

ISSN
1948-7185

Authors
Ahmed, Musahid
Lu, Wenchao

Publication Date
2023-10-19

DOI
10.1021/acs.jpclett.3c02263

Probing Complex Chemical Processes at the Molecular Level with Vibrational Spectroscopy & X-Ray Tools

Musahid Ahmed[1]* and Wenchao Lu[1,2]

[1] Chemical Sciences Division, Lawrence Berkeley National Laboratory, Berkeley, CA 94720, USA

[2] CSIRO Environment, Urrbrae, SA 5064, Australia

mahmed@lbl.gov

TOC Graphic

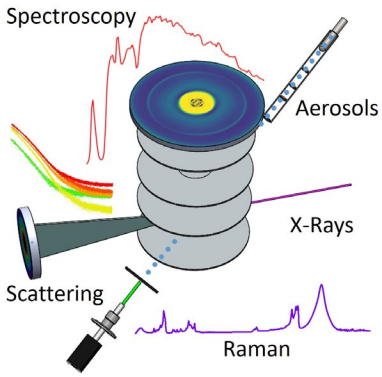

Abstract:

Understanding the origins of structure and bonding at the molecular level in complex chemical systems spanning magnitudes in length and time are of paramount interest in physical chemistry. We have coupled vibrational spectroscopy and X-ray based techniques with a series of micro-reactors and aerosol beams to tease out intricate and sometimes subtle interactions, such as hydrogen bonding, proton transfer, and non-covalent interactions. This allows for unraveling the self-assembly of arginine-oleic acid complexes in aqueous solution and growth processes in a metal-organic framework. Terahertz and Infrared spectroscopy provide an intimate view of the hydrogen-bond network and associated phase changes with temperature in neopentyl glycol. The hydrogen-bond network in aqueous glycerol aerosols and levels of protonation of nicotine in aqueous aerosols are visualized. Future directions in probing the hydrogen-bond networks in deep eutectic solvents and organic frameworks are described, and we suggest how X-ray scattering coupled with X-ray spectroscopy can offer insight into the reactivity of organic aerosols.

The dynamics of complex and typically heterogeneous systems have long captured the attention of the physical chemistry community, owing to their prevalence in natural processes and inherent complexity. Heterogeneous systems play crucial roles in solvation, micro-confinement, crystallization, self- and supramolecular assemblies, interfacial dynamics and structural relaxation, among many other processes.[1] These areas represent some of the most fundamental topics in chemistry and are extremely relevant to study if we seek to decarbonize our energy sources and live in a sustainable way in the future. In nature, these processes are driven both by non-covalent interactions such as van der Waals forces and hydrogen bonds and by covalent bonds.[2] For example, non-covalent interactions and hydrogen bonding are deeply implicated in numerous processes in soft systems, crystals, and liquids. These interactions are critical for maintaining the structural integrity and stability of macromolecules, such as proteins and polymers,[3] which further provide a versatile toolbox for tuning the structural, morphological, and functional properties of materials and systems. Covalent bonds, on the other hand, dominate in the formation of various skeletons and backbones of products, ranging from inorganic minerals to organic compounds and biological macromolecules. Understanding and controlling covalent bonds are essential in the thermodynamics and kinetics for fine-tuning the formation of complex morphologies, and have a significant impact on the functionalization of the resulting materials.[4]

Despite their importance, the fundamental principles governing these processes remain challenging to elucidate and are often debated due to their intricate nature. In addition to bulk measurements, a molecular-level view is often necessary. In recent studies, scientists have not only focused on static analysis for systems at equilibrium but have also become increasingly interested in examining the dynamics of non-equilibrium heterogeneous systems.[1] Thanks to the advancements in spectroscopic techniques bolstered by high-level computational work, modern technologies now permit an in-depth, molecular-level understanding of physicochemical processes in heterogeneous systems. Spectroscopy can investigate various interactions and chemical bonds depending on the photon energy, allowing scientists to employ multiple techniques to extract structural information from various perspectives. Here we describe our modest efforts in coupling vibrational spectroscopy to soft X-ray photoelectron and absorption spectroscopy to probe these processes at the Advanced Light Source (ALS), a synchrotron facility located at Berkeley Lab. The colocation of hard X-ray scattering apparatus at this facility allows for the coupling of small and wide-angle X-Ray scattering to vibrational spectroscopy.

Terahertz (THz) and far-infrared (FIR) spectroscopies operate in the 0.1 – 20 THz (3.3 – 670 cm^{-1} in wavenumber) range and are highly sensitive to non-covalent interactions, providing fingerprint information

of molecules and structures, and making them ideal for probing systems reliant on structural reorganizations driven by intermolecular Coulombic forces.[5, 6] Mid-infrared (MIR) spectroscopy, operating between 600 – 4000 cm^{-1}, can identify formation and breaking of covalent bonds, as each type of bond vibration or rotation exhibits characteristic absorption peaks at specific wavenumbers. Peak shifts caused by chemical environment change allow the use of IR spectroscopy for studying non-covalent interactions, particularly O-H stretching within hydrogen-bond networks.[7] Soft X-rays, with energies ranging from 10^2 – 10^3 eV, are capable of deciphering electronic structure in exquisite detail. X-ray photoelectron spectroscopy (XPS) provides a surface-sensitive probe while near-edge X-ray absorption fine structure (NEXAFS) is sensitive to the bulk concentration. XPS provides information via binding energy (illustrates changes in the bonding environment) and the intensity (signifies a quantitative understanding of each component present on the surface), and NEXAFS provides information about different types of hydrogen bonding. Besides NEXAFS, there are also absorption- and emission-based soft X-ray spectroscopies such as extended X-ray absorption fine structure (EXAFS) and X-ray emission spectroscopy (XES). Similar to NEXAFS, EXAFS measures the absorption of X-ray photons that causes the ejection of a core electron. XES on the other hand, measures the X-ray photons emitted when such an electron hole is refilled by another electron. Both EXAFS and XES can assess the bonding and coordinating environment of an atom, however we have chosen to work with XPS and NEXAFS since our access to X-ray photons is limited to less than 1 keV. Hard X-rays, with energy ranges up to 10^4 eV, are particularly useful in small- and wide-angle X-ray scattering (SAXS/WAXS) studies to investigate crystalline structure at the nanoscale and we have adapted our experiments to access these ranges at the ALS.[8] In the cases described here, multiple spectroscopy techniques are used when investigating a system to acquire comprehensive insights into the chemical environment. We note that there are many other methods available to probe heterogeneous processes both in an *in situ* and multimodal manner, and we point the interested reader to these comprehensive reviews.[9, 10] Methods such as neutron scattering[11] & NMR spectroscopy[12] have been deployed to probe heterogeneous processes and in this perspective we compare two examples of using such methods when describing phase changes in a plastic crystal[7] and reactivity in a Diels Alders reaction,[13] respectively.

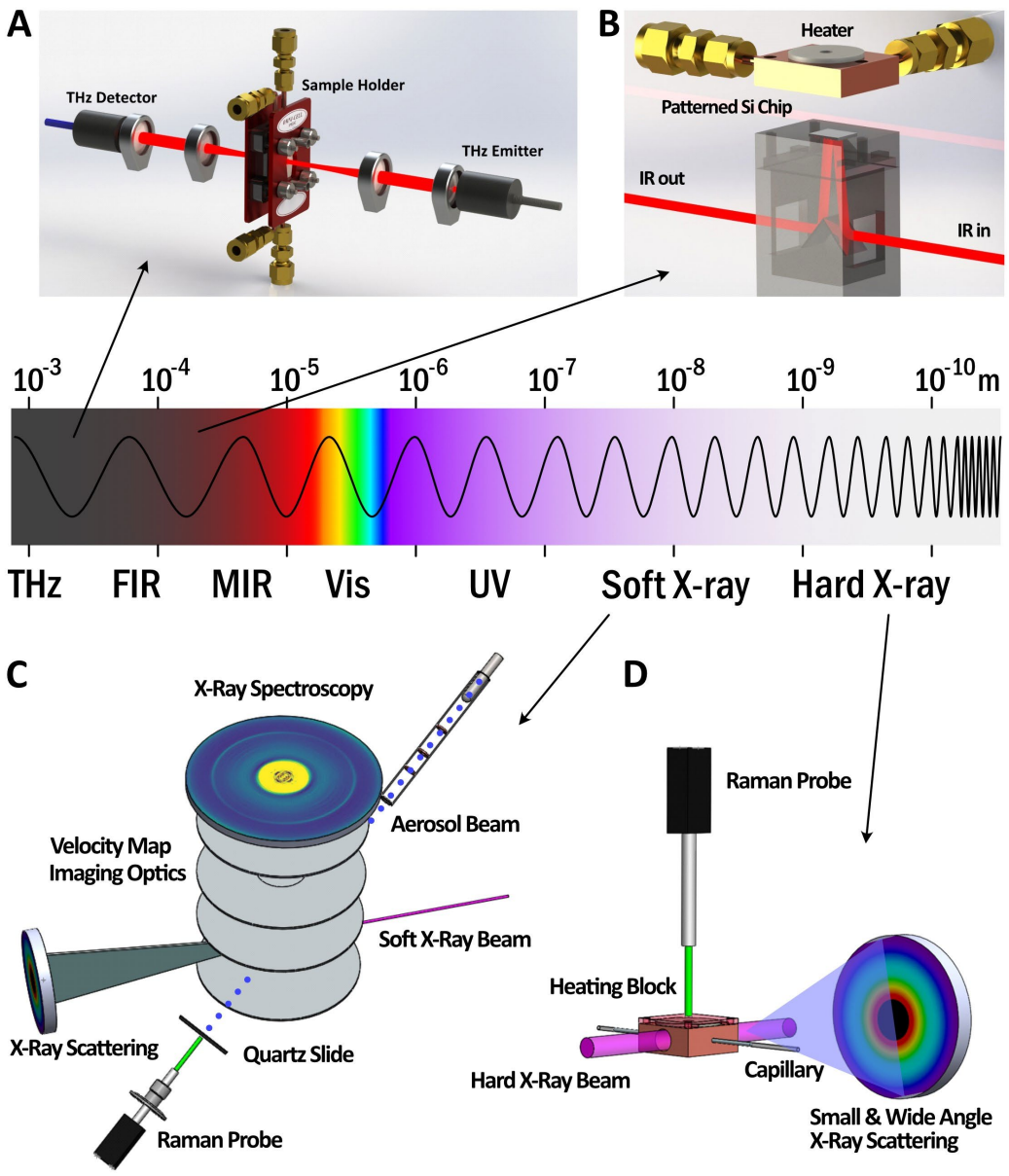

Figure 1. An overview of the spectral band and related experimental tools used to probe the systems described in the present perspective. (**A**) THz time-domain spectroscopy coupled to absorption through a Teflon/quartz window in a Specac cell that has been adapted for measuring phase changes with temperature & chemical reactions. (**B**) A microfabricated Si-based ATR chip reactor that is used to perform temperature-dependent studies on chemical reactions, molecular growth processes & phase changes. (**C**) An aerosol apparatus coupled to a soft X-ray beamline at the ALS used to perform X-ray spectroscopy and scattering together in in-situ Raman spectroscopy to study solvation, proton transfer and hydrogen bonding. Also shown is a quartz slide on which aerosols are deposited within the spectrometer and probed via Raman spectroscopy. (**D**) A capillary-based heated reactor incorporated into a hard X-ray beamline at the ALS to

study phase changes, nucleation, and crystallization with SAXS/WAXS coupled to in-situ Raman spectroscopy.

At Berkeley Lab, our team has successfully developed a series of micro-reactors integrated with both synchrotron- and non-synchrotron-based spectroscopic techniques (**Fig. 1**), to establish a molecular-level understanding of the dynamics in heterogeneous systems. Our experimental setup includes a commercial THz system (Tera K15, Menlo Systems), a Bruker VERTEX 70 FTIR spectrometer with a silicon-based attenuated total reflection (ATR) device (IRUBIS) for MIR and FIR measurements, and various fiber coupled probes at 532 nm for Raman spectroscopy measurements.[7, 14] Our spectroscopic measurements benefit from the ALS synchrotron facility, including a soft X-ray velocity map imaging (VMI) spectrometer at Beamline 9.0.1,[15] as well as micro-reactors interfaced to the SAXS/WAXS beamline using 10 keV monochromatic X-rays at Beamline 7.3.3.[8] Our experiments are bolstered with *ab initio* computational analysis when possible. By integrating these state-of-the-art techniques and approaches, we have established a robust and versatile platform for achieving an unprecedented molecular-level understanding of a variety of systems described in this perspective.

Hydrogen-bonded systems in condensed phase

Self-assembly of biomolecules. Self-assembly generally involves multiple steps; although fast equilibria are challenging to monitor, slow rate-determining steps can be readily tracked using the aforementioned spectroscopies combined with computational approaches. Arginine (Arg), an amino acid, was investigated as a prototype molecule to study these processes, since it has a flexible molecular structure with a guanidinium head group and an alpha amino acid tail concatenated by a hydrocarbon backbone. The first example is the self-assembly process of Arg and oleic acid (OA), shown in **Fig. 2A**.[6] The guanidino group in Arg facilitates the formation of molecular Arg-OA pairs through hydrogen bonds.[16] While most spectroscopic techniques used to investigate the self-assembly processes emphasized their functionality, such as characterization, morphology, crystallography, and pH- and concentration-dependence, few studies have approached these systems from a kinetic perspective, especially when the system is far from equilibrium.

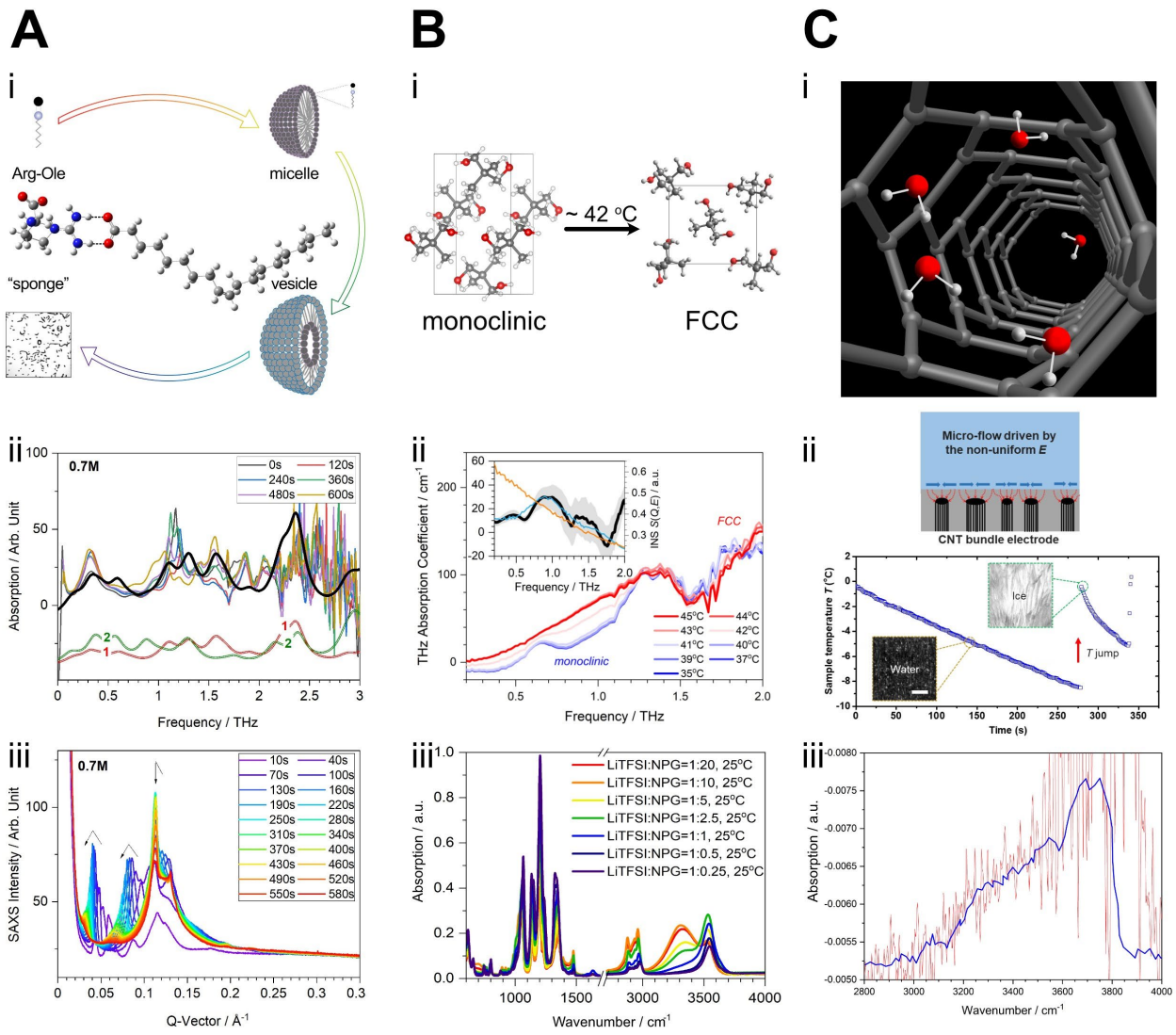

Figure 2. (**A i**) Schematic depicting the self-assembly process of Arg-OA aqueous solution; (**A ii**) THz spectra collected for the first 10 minutes at the Arg-OA interface of 0.7 M pH = 11 arginine solution. The red and green curves are the calculated THz spectra of the 2 lowest-lying conformers and the black thick curve is the linear combination of the 2 calculated spectra weighed by their populations at 298K; (**A iii**) SAXS spectra collected during the first 10 minutes at the Arg-OA interface. The black arrows in each frame indicate the position change of each peak. Adapted from Ref. 6. Copyright 2020 American Chemical Society. (**B i**) The crystal lattices of monoclinic and FCC NPG; (**B ii**) THz spectra, showing the solid-to-solid phase change at 41°C. The inset shows the THz absorption difference between monoclinic and FCC NPG in comparison to inelastic neutron scattering dynamic structure factor of monoclinic (azure) and FCC (orange) NPG from Ref. 17; (**B iii**) The IR spectra when doping with different proportions of LiTFSI salt. Adapted from Ref. 7. Copyright 2022 Cell Press. (**C i**) Water uptake within a carbon nanotube; (**C ii**) The proposed mechanism

and the temperature-time curve measuring the onset of freezing using a customized electrowetting system. Inset pictures are the sample in liquid and solid phases during the experiment, and the scale bar is 2 mm. Adapted from Ref. 18. Copyright 2020 American Chemical Society; (C iii) Preliminary ATR-FTIR measurement of a fully hydrated carbon nanotube (red) compared to the work by Dalla Bernardina et al. (blue)[19]. The signal beyond 3700 cm^{-1} is due to gas-phase water.

Previous studies have suggested that the self-assembly process of arginine and fatty acids (FA) is favored under strong basic conditions.[20, 21] The proposed mechanism begins with the formation of Arg-FA pairs, which self-assemble into micelles. These micelles continue to grow into multi-layered vesicles and ultimately aggregate into sponge-like structures.[20, 21] Utilizing THz and SAXS (Fig. 2A ii and iii), we have re-investigated the self-assembly of Arg and oleic acid (OA), a C_{18} fatty acid.[6] Our study focused on the initial 10 minutes when sponge-like aggregates rapidly accumulated in the solution. During this period, conditions within the reactants are far from equilibrium and are diffusion-controlled. The SAXS results suggested that the formation of Arg-OA pairs and micelles is via a fast equilibrium. The successive build-up process into vesicles is observed in the SAXS spectra, with aggregate sizes reaching up to 200 Å. Previous scanning electron microscope investigation reveals that various-sized vesicles co-exist in the system.[21] These seed aggregates serve as building blocks for constructing larger-scale sponge-like structures, held together by hydrogen-bond networks involving water molecules. The final product is very stable and is not affected in strong acidic and basic environments.[6] While we used density functional theory (DFT) calculations to support our experimental results, we note that calculating THz spectra using single-molecule representation is notoriously challenging, particularly for solid crystalline states due to the insufficiently accurate treatment of weak intermolecular interactions.[22] Nevertheless, the resemblance between the calculated and experimental THz spectrum did suggest that the self-assembly aggregates exhibit a loosely bound structure without a repetitive crystal lattice pattern having strong intermolecular interactions. Also, this intrinsic structural difference in Arg-OA aggregates renders solid-state calculations unsuitable.

Hydrogen-bond network in a plastic crystal. Hydrogen bonds are a subset of non-covalent interactions that exist when a highly electronegative atom attracts a hydrogen atom that is bonded to another electronegative atom ($A^{\delta-}$-$H^{\delta+}\cdots\cdots$B). Often considered as weak interactions, water hydrogen bonds possess dissociation energies of approximately 3 – 5 kcal/mol, while the strongest one can reach 40 kcal/mol.[23] Prior experimental investigations have employed X-ray diffraction (XRD)[24] and inelastic neutron scattering (INS)[25] to examine hydrogen-bond networks. THz spectroscopy, due to its sensitivity to weak interactions,

is frequently employed to explore energetic processes and dynamics therein. Furthermore, hydrogen-bond networks affect not only the $A^{\delta-}$-$H^{\delta+}$ bond (e.g., O-H and N-H bonds) but also the rovibrational modes, and thus cause peak shifts in IR spectroscopy.[25] This sensitivity to rovibrational modes makes IR spectroscopy an effective method to directly probe the hydrogen-bond network within condensed systems such as polyols and water. Neopentyl glycol (NPG), a polyalcohol and also a plastic crystal, has recently garnered attention due to its remarkable barocaloric effects and associated possibility for thermal energy storage.[26] NPG undergoes a solid-solid phase transition from monoclinic to face-centered cubic (FCC) at 41 – 42°C (**Fig. 2B i**),[26] which can be visualized via THz and IR spectra (**Fig. 2B ii**).[7] Notably, the THz absorption difference between monoclinic and FCC NPG mirrors the dynamic structure factor of these two phases as determined by INS, providing an inexpensive and accessible measurement of the phase transition.[7, 17]

The hydrogen-bond network within NPG is significantly attenuated upon mixing with lithium bis-(trifluoromethane)sulfonimide (LiTFSI),[7, 27] a salt commonly employed in Li-ion batteries. **Fig. 2B iii** presents the IR spectra of NPG/LiTFSI mixtures across a range of molar ratios from 20:1 to 0.25:1. The IR spectra reveal not only the alterations in the overall spectral profiles but also the specific changes in the O-H bonds as the concentration of LiTFSI increases. This can be attributed to the less nucleophilic nature of the $TFSI^-$ anion, which arises from charge dispersion induced by the presence of strong electron-withdrawing perfluoroalkyl sulfonyl groups. The $TFSI^-$ anion efficiently disrupts the crystal lattice, leading to the structural change from the freed NPG monomers to an intramolecularly H-bonded steric conformer. This, in turn, results in noticeable changes to the spectral details. A close examination of the O-H stretching peak reveals the emergence of intramolecular O-H bonds at approximately 3550 cm^{-1}, as opposed to the intermolecular bonds predominantly observed in pure NPG crystals. An analysis of *n*(LiTFS)% vs. the absorption of O-H stretching around 3550 cm^{-1} identifies a turning point at *n*(LiTFS)% ≈ 30 % (equivalent to NPG:LiTFSI = 2.5:1 in molar ratio), which signifies the highest efficacy of LiTFSI in restructuring the hydrogen-bond network. Interestingly, the O-H stretching peak for highly concentrated LiTFSI mixtures exhibits contributions from free O-H stretching even in the absence of intramolecular hydrogen bonds. This finding reveals the complex and versatile role of LiTFSI in modifying the hydrogen-bond network within condensed-phase polyalcohol systems.[7] Notably, DFT calculations for spectroscopy primarily elucidate rovibrational modes associated with covalent bonds, potentially neglecting subtle peak variations influenced by hydrogen-bond networks. Nevertheless, a single-molecule representation in DFT calculation, as opposed to crystal calculations, maintains its utility in facilitating the peak assignment of IR spectra.

Ice nucleation. Water freezing is important in the natural world pertaining to climate change, sea level change and crucially relevant in many industrial applications. While effective control of ice nucleation (nucleation temperature, nucleation rate, ice crystal size, etc.) under different environmental conditions is highly desirable,[28] in reality it has proven to be incredibly challenging. Nucleation of ice involves a synergy of weak interaction-based phase change and external complications such as supercooling,[29] which renders its effective control difficult. Ice nucleation can be facilitated and controlled by electric fields both in bulk and in confinement.[30] Previously, simulation and experiment were performed to investigate the ice nucleation by changing the thickness of a carbon nanotube (CNT)-based dielectric layer and voltage, and the results indicate a possibility to tune the freezing temperature by varying the electric field (**Fig. 2C i and ii**).[18] However, a molecular-level understanding especially the interfacial mechanisms in an electric field is missing in conventional studies. Fortunately, water in different states can be easily disentangled by vibrational spectroscopy. A hydrogen-bonding environment can cause peak shift and deform the vibrational modes of O-H bonds, and thus vibrational spectroscopy can be used to explore the hydrogen-bond network affected by external factors. A recent study shows that water uptake in CNTs with diameters from 0.7 to 2.1 nm has a combination of different types of phase behavior, such as bulk water, ice, loosely-bound water, etc. using synchrotron-based IR spectroscopy.[19] In the future, we plan to couple our existing silicon-based ATR device to microfluidics, electrodes, and heating/cooling elements, and mount it to conventional FTIR, broadband THz, and IR lasers for a comprehensive description of the hydrogen bonding of water and associated phase changes upon electrification.[31] The new ATR-based apparatus can also explore the effects of local electric fields. Our preliminary ATR-FTIR results show similar water uptake behaviors in hydrated CNT compared to that measured in the literature, with the benefit that these measurements were performed with a benchtop FTIR and did not require the use of synchrotron-based FTIR (**Fig. 2C iii**).

Reactions in microscopic confinement

Growth of metal-organic frameworks in aqueous solution. Metal-organic frameworks (MOFs) are becoming increasingly attractive for scientists due to their chemical tunability and high internal surface area.[32] These crystalline materials are comprised of metal ions connected by organic linkers to form porous structures that can be optimized for a particular purpose, promising a world of molecular-level "crystal engineering."[33] However, the synthetic principles behind MOF formation are still in the tinker-and-see stage, and more often than not rely generally on brute force strategies such as high-throughput screening and trial-and-error.[34] MOF syntheses are described by complex free energy landscapes that determine correlated atomic

and molecular motions over multiple length and time scales. Active kinetic control of emergent behavior within these systems requires detailed understanding of structural transformation, reaction, and diffusion kinetics on the system-relevant length and time scales. Hence, we employed a multimodal approach encompassing wide-angle X-ray scattering (WAXS), Raman spectroscopy, mid-infrared (MIR) spectroscopy, and far-infrared (FIR) spectroscopy to investigate the growth kinetics of Co-MOF-74 across various length scales using microscopic volumes of reagents confined either in a capillary or a chip-based reactor.[14] WAXS and FIR spectroscopy provided details about the atomic coordinates and lattice of the MOF, while Raman and MIR spectroscopy provide molecular information on the linker modes. Plane wave density functional theory was used to calculate Raman, FIR, and MIR spectra, to assign modes to the experimental spectra, and to provide a molecular structural view of the MOF. The growth curves of nucleation extracted from the scattering and spectroscopy measurements are compared to earlier reports in the literature.

We synthesized and analyzed the Co_2(dobdc) system (dobdc^{4-} = 2,5-dioxido-1,4-benzenedicarboxylate, Co-MOF-74) within a sealed micro-reactor of 200 µL volume mounted *in-situ* on an ATR device (**Fig. 3A i**).[14] IR spectra (**Fig. 3Aii**) are collected to investigate bonding formation whereas FIR and SAXS/WAXS to elucidate the information of the hexagonal crystal lattice, with the support of crystal calculations. Several IR spectral changes were observed, including 580 cm^{-1} for Co–O stretching (**Fig. 3A ii**) and other peaks from 1100 – 1600 cm^{-1} for carbon backbone bonding stretching. The kinetic traces of Co–O stretching absorption (**Fig. 3A iii**) against reaction time at different temperatures visualize the kinetics of nucleation and crystallization. We used a mathematical model, developed by Gualtieri et al. to parameterize zeolite growth kinetics,[35] for simulating crystallization and separating the nucleation and growth rate constants. Utilizing this model,[35] the extracted activation energies of 102.0 kJ mol^{-1} for nucleation and 138.7 kJ mol^{-1} for growth are significantly higher compared to bulk-solution growth kinetics (66.5 and 90.4 kJ mol^{-1} for nucleation and growth, respectively) measurements by Osta et al.[36] When reducing the volume down to 100 µL, the reaction rate accelerates even further. We hypothesize that the accelerated reaction rate stems from reactants reaching the surface of the ATR chip more rapidly as the volume decreases. Since heterogeneous nucleation occurs at sites on surfaces, the ATR chip on the bottom likely serves as a nucleation site, promptly detecting the newly formed Co-MOF-74 crystals. Meanwhile, we found that the morphology of Co-MOF-74 crystals was highly uniform, with an average size of approximately 2 µm, which is smaller compared to previous studies.[36-38] These results suggest that not only the reaction kinetics but also morphology within micro-confined systems may vary significantly from in-bulk conditions. The influence of solvents (e.g., water) and confinement on accelerating and catalyzing chemical reactions is a very interesting topic to investigate further and we suggest future directions in the next section.

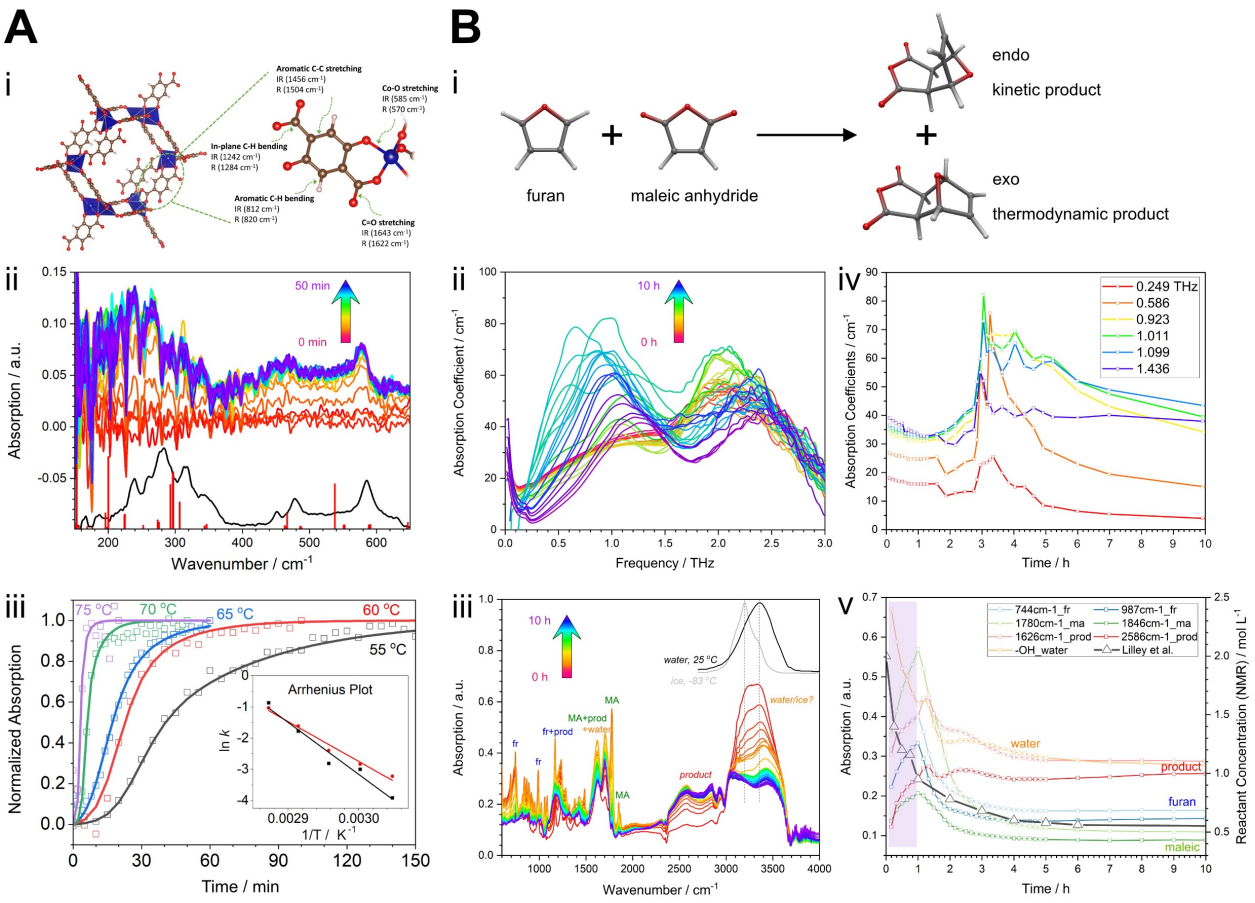

Figure 3. (**A i**) A molecular representation of the Co_2(dobdc). The red balls represent oxygen atoms, brown for carbon atoms, pale pink for hydrogen atoms, and blue for cobalt atoms. Also shown are the linker molecule and the relevant vibrational modes for Raman and IR spectroscopy; (**A ii**) ATR-FIR time-dependent data collected from a chip-based reactor at a heater temperature of 70 °C. The black spectrum is from MOF crystals formed on the chip after all solvent has been evaporated off, while the red sticks are from a plane wave density functional calculation scaled by a factor of 1.1; (**A iii**) A kinetic model fitting based on the 580 cm^{-1} peak at 55, 60, 65, 70, and 75°C. The inset shows the corresponding Arrhenius plot where the activation energies of nucleation (red) and growth (black) can be extracted. Adapted from Ref. 14 with permission from the Royal Society of Chemistry. (**B i**) The Diels-Alder reaction of furan and maleic anhydride with water added to the system, measured by (**B ii**) THz spectroscopy and (**B iii**) ATR-FTIR. The IR spectra of water at 25 °C and ice at -83 °C, extracted from Ref. 39 are also shown with the peak positions marked by gray dashed lines. The kinetic traces on the right show the evolution of several feature peaks over time for (**B iv**) THz and (**B v**) FTIR, with the reactant concentration kinetics measured by Lilley et al. using NMR.[13]

Reactivity within confinement. Recently, "active matter" has been discussed as a topic of interest in the physical chemistry community and experimental reports have emerged where molecular mobility has been claimed to be "boosted" in chemical reactions.[40] Furthermore, the role of solvent (water) and confinement to accelerate or catalyze reactions has also been discussed.[41] The Diels-Alder reaction between furan and maleic anhydride is moderately exothermic and entropically disfavored (ΔG is only a few kcal/mol), and therefore can be easily influenced by external changes such as different types (such as in water, DMSO, diethyl ether, etc.) and amounts of catalytic solvents. This provides a rich environment to probe the Diels-Alder reaction as a model for active matter dynamics with experiment and test with theory. Indeed, these classes of cycloaddition reactions have also been suggested for the storage of thermal energy in bonds due to their enhanced heat capacity. By their nature, cycloaddition reactions possess both a high ΔH (providing large heat capacity enhancement) and high ΔS (necessary to ensure reactions occur at practical temperatures), making them uniquely suited to the task and affording a large design space.[13] We chose to investigate the classic Diels-Alder reaction between furan and maleic anhydride (**Fig. 3B i**) using our micro-reactors coupled with vibrational spectroscopies. Before measurements, 0.15g of maleic anhydride (≥ 99.0%, Sigma-Aldrich) was first dissolved in 1.0 mL of furan (≥ 99.0%, Sigma-Aldrich). Successively, 300 µL of the resulting clear solution and 100 µL water were added to the micro-reactor. Our preliminary THz and IR results reveal the reaction kinetics intertwined with diffusion (**Fig. 3B ii** and **iii**). Three stages can be distinguished from the kinetic trace of each peak (**Fig. 3B iv** and **v**). The first stage is usually smooth until a "turning point" appears at about 1 – 2 hr in IR and 3 – 4 hr in THz spectra. Lilley et al. have also investigated the reaction kinetics using NMR.[13] Our kinetic measurements of maleic anhydride via IR (**Fig. 3B v**) follows the similar depletion kinetics of reactant measured by NMR. However, in our system, a slight retardation caused by diffusion occurs at the first hour whereas no diffusion was observed over the course of reaction from NMR measurements. Earlier studies reported that significant diffusion occurs especially at the initial stage of reactions.[40] Since furan is not miscible with water, the diffusion may exhibit more complex behaviors. The faster kinetics observed from IR than THz was due to the fact that ATR monitors the bottom of the reactor where water micro-droplets aggregate, causing stronger diffusion and associated catalytic effects. Future work will investigate the hydrogen-bond networks and the dynamics under different types and amounts of catalytic solvents to visualize the overall reactivity influenced by the diffusion of the system.

Probing aerosols with X-ray spectroscopy, vibrational spectroscopy and X-ray scattering

Hydrogen-bond networks in aqueous glycerol aerosols. The hydrogen-bond network within a composite system implicates co-solvation and may exhibit significant differences from pure substances, depending on the concentration of each component. We focus our efforts on using poly-alcohols, particularly glycerol, to develop an understanding of the molecular heterogeneities that occur upon their interaction in aqueous co-solvent systems.[42] These poly-alcohols show significant deviation from ideal behavior upon mixing with solvents, and ions in the bulk environment which is directly a result of micro heterogeneity and liquid-liquid phase separation and solid-solid phase changes, respectively. This complex behavior provides a rich tapestry to test hydrogen bond dynamics, probe solvation and confinement, and map nucleation and crystallization events.

There have been many experimental and theoretical attempts to understand the mechanistic details of the hydrogen-bond network upon mixing glycerol with water. However, a molecular-level picture of glycerol water mixtures, particularly in aerosols, remains opaque. To visualize the hydrogen-bond network of glycerol-water aerosols, we used velocity map imaging X-Ray photoelectron spectroscopy (**Fig. 1C**) pioneered in our group to study solvation, proton transfer and chemical reactivity.[43] Since oxygen is present in both water and glycerol, by comparing the O 1s XPS spectra with C, we will disentangle the contributions of water and glycerol to the hydrogen-bond network. The molecular heterogeneities that occur in the associated solutions from which these aerosols are generated were connected at the structural level by coupling the XPS results to a chip-based ATR-FTIR and THz time-domain spectroscopy analysis. The C 1s and O 1s X-ray photoelectron spectra at different glycerol water concentrations are shown in **Fig. 4A**. In the C XPS spectrum, a broad peak is observed between 296-287 eV which should be representative of the glycerol content of the aerosol beam, whereas a similar broad peak is observed between 542-534 eV at the oxygen spectrum and its contribution is from both glycerol and water. The contributions to these peaks will arise from the gas and condensed phase components of the mixture. In **Fig. 4A**, we fitted the experimental data with two Gaussians to represent the gas (292 eV) and condensed phase (290.5 eV) component and the sum shows the fit to the experimental data reasonably well. Our analysis is in good agreement with both experimental[44] and theoretical literature[45] in the case of binding energy shifts and peak positions (540 and 538.5 eV) shown in the 1 mol% data (almost completely water) of the O 1s spectrum. By obtaining the amplitudes of the peaks shown by the Gaussian distributions in **Fig. 4A**, we can extract the changes in the condensed phase contributions at the C and O 1s levels respectively as a function of concentration. In the C distribution, the intensity shows a sharp rise from 1 mol% to 23 mol% and then gradually drops down in intensity to 78 mol% concentration. In the O intensity distribution, the peak rises steadily between 1 – 9.5 mol%, drops at 16 mol%, then a small rise until 23 mol% and then continues to drop in intensity. The

intensity drop at higher glycerol concentration is due to enhanced evaporation of the glycerol molecules and upon water addition, results in mutual depression of vapor pressures slowing down the evaporation.

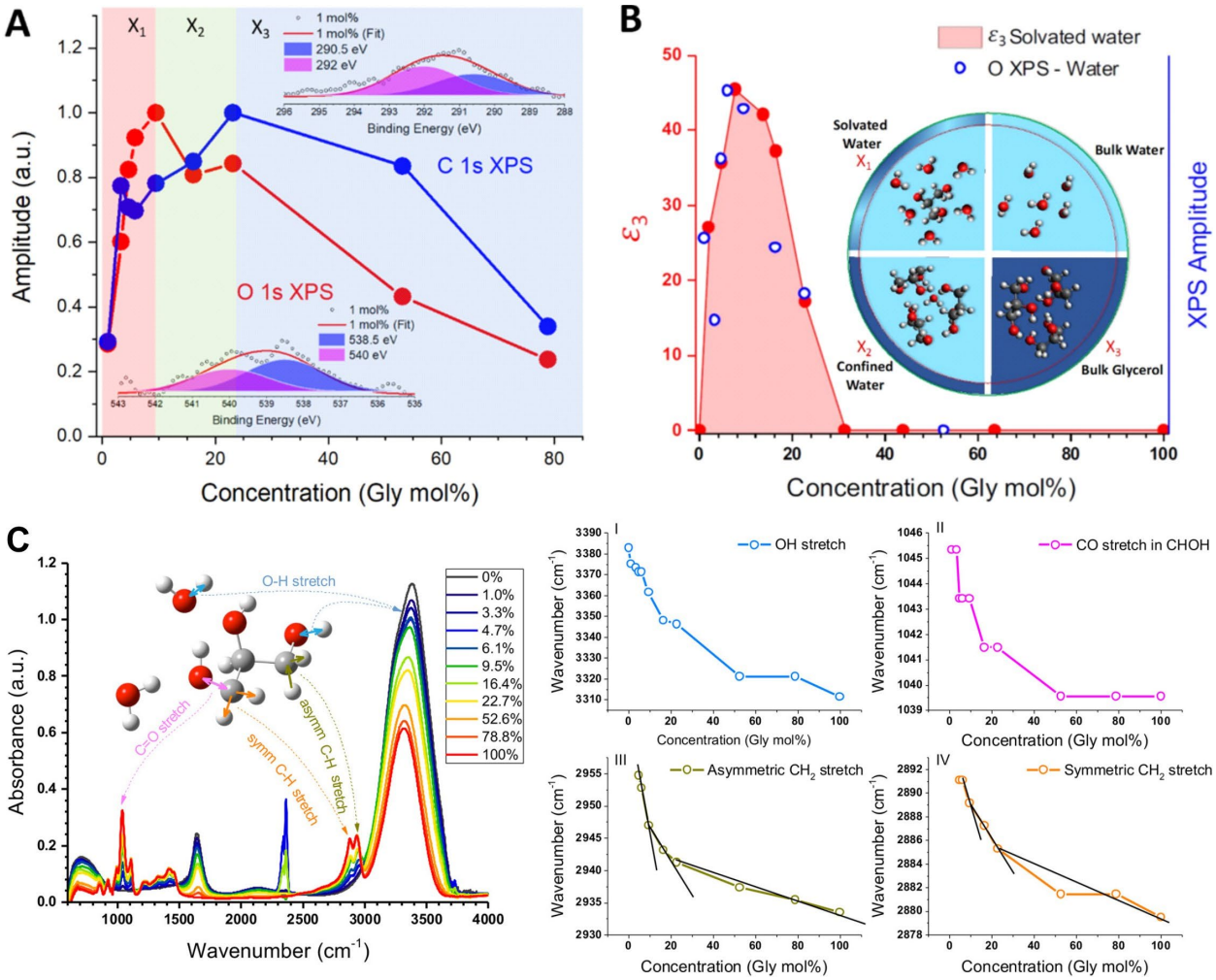

Figure 4. (**A**) Condensed-phase C and O XPS intensities as a function of glycerol mol%. The insets show the C 1s and O 1s XPS peak intensities. Three regions corresponding to glycerol-water networks are indicated in colored regions, red (X1) is solvated water, green (X2) is confined water and blue (X3) is bulk glycerol network. (**B**) Comparison of dielectric relaxation trend for solvated water (ε_3) with O 1s XPS intensities of water extracted by normalizing total O signal from C signal. Also shown is a representation of the four types of hydrogen-bond networks identified using a combination of X-ray, THz and FTIR spectroscopy. (**C**) ATR-IR spectra obtained for different glycerol–water concentrations. Also shown are wavenumber trends for four vibrational modes: (I) OH stretching band, (II) CO stretching, (III) asymmetric CH2 stretching, and (IV) symmetric CH2 stretching. Adapted from Ref. 46. Copyright 2021 American Chemical Society.

The C intensity distribution has one prominent peak at 23 mol% and that of O shows two peaks at 9.6 mol% and 23 mol% which could be due to changes in the hydrogen-bond network. Similar trends were observed in a dielectric and THz study performed by Vinh and coworkers,[47] in aqueous solutions of glycerol. We performed parallel THz and IR measurements which corroborate and set the stage for the description of the hydrogen-bond network observed in the mixtures. Considering the bulk water system where all hydrogen bonding is between water molecules, adding glycerol results in their accumulation in the hydration layer. Since each glycerol can bond with 6 water molecules, the number of waters in the hydration layer also gradually leads to a formation of a layer of solvated water. From dielectric relaxation calculations, a critical glycerol concentration of ~7.5 mol% was obtained as the maximum number of water molecules in the hydration layer,[47] whereas in the O 1s XPS, the first major feature observed at 9.5 mol% probes this solvated water network (region X_1 in **Fig. 4A**). Adding more glycerol into the mixture, results in water being replaced by glycerol molecules forming predominantly a network of glycerol with confined water (region X_2). A second, less intense feature observed at 23 mol% is attributed to this glycerol-water network. The low intensity of the signal can be explained by having the O atom contribution only from glycerol, since water is embedded inside the glycerol cluster and XPS is only sensitive to the surface. For the C XPS intensity, the peak at 23 mol% matches with O XPS intensities further justifying our explanation. After, 23 mol%, at high glycerol concentrations, the system mostly behaves as bulk glycerol (region X_3) and the O XPS intensity gradually decreases due to low number density of the aerosol particle owing to evaporation.

We performed THz-TDS measurements of the glycerol water solutions to discern the hydrogen-bond network patterns suggested by the XPS analysis and dielectric studies mentioned in the literature.[47] According to the dielectric trends, solvated water peaks at 7.8 mol% and confined water peaks at 31 mol% is in excellent agreement with the two features observed in the XPS results. As XPS is sensitive to the surface layer of the aerosol, contributions to the condensed phase signal of water in O 1s XPS can only arise from solvated water. Thus, ε_3 dielectric constant of solvated water and pure water O XPS intensities should have a similar distribution. The O condensed phase signal has contributions from both pure water and glycerol, and only glycerol will contribute directly to the C XPS signal. Therefore, to extract the trend of water contribution to O 1s XPS signal, the O XPS intensity distribution was divided by the C XPS intensity distribution. As shown in **Fig. 4B**, almost a perfect match is observed, demonstrating a correlation between the XPS and THz measurements. A molecular picture correlated with this dielectric analysis emerges by

probing the glycerol water mixture with ATR-FTIR spectroscopy (**Fig. 4C**). Short hydrogen bonds are formed between water with inner CHOH and outer CH_2OH groups of glycerol while long hydrogen bonds are formed with outer CH_2OH groups. At high concentrations, more intermolecular interactions are formed between glycerol molecules and spectroscopy indicates bonds are formed between the H of CH_2 groups and the O of COH groups. Three regions are identified through changes in the CH_2 spectra: In the first region (4 – 9.5 mol%), glycerol is solvated by water and backbone CH_2 groups can form weak CH---OH bonds. In the second region (9.5 – 22.7 mol%), weakening of the hydrogen bonding caused by water being replaced by glycerol molecules in the confined water network is observed. At this point, water tends to bond more with the glycerol hydroxyl group and weaker glycerol OH groups form interactions with the alkyl backbone. Finally, a smaller change is seen by adding more glycerol into the system forming glycerol clusters in the bulk glycerol network.

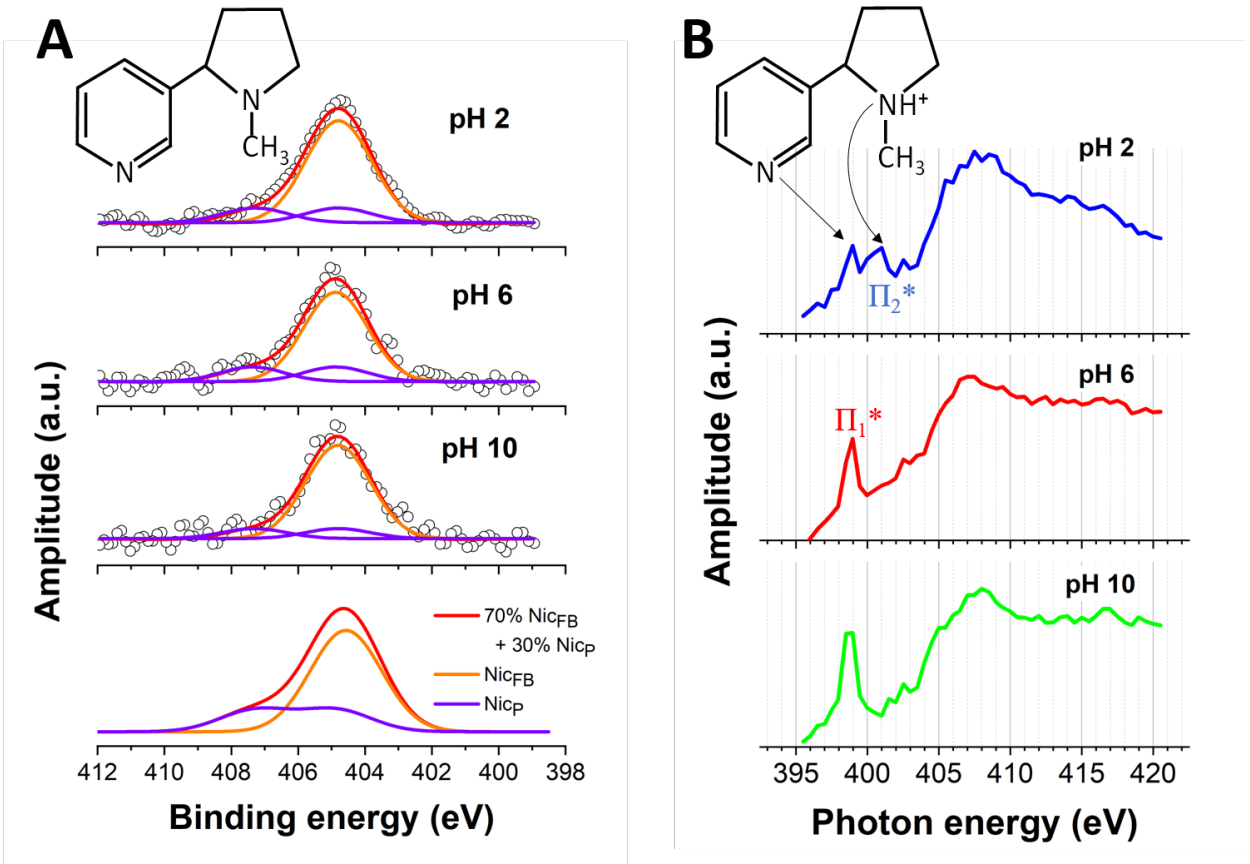

Figure 5. (**A**) N 1s XPS spectra of aerosols generated by nebulizing aqueous solutions containing 0.5 M nicotine at pH 2, pH 6, and pH 10.4. The black line is the experimental spectra, and the dashed red line is a

convolution of the free-base (orange) and protonated (purple) nicotine. The bottom panel corresponds to DFT-calculated spectra for free-base nicotine (Nic_{FB}), protonated nicotine (Nic_{P}) and a 70%/30% combination thereof. The DFT values are shifted by 1.8 eV on the absolute scale to overlap with the experimental results. (B) N K-edge NEXAFS spectra of aerosols generated by nebulizing aqueous solutions containing 0.5 M nicotine at pH 2, pH 6, and pH 10.4. Adapted from Ref. 48. Copyright 2023 American Chemical Society.

X-ray spectroscopic analysis of nicotine protonation in aqueous aerosols. A new generation of electronic cigarettes is exacerbating the youth vaping epidemic by incorporating additives that increase the acidity of generated aerosols, which facilitate uptake of high nicotine levels. We need to better understand the chemical speciation of vaping aerosols to assess the impact of acidification. The extent of nicotine protonation in the aerosol particles was determined by XPS and NEXAFS, which allows for interrogation of the aerosol surface and the particle core, respectively. To investigate the effect of protonation, solutions of aqueous nicotine 0.5 M at pH 10.4, 6, and 2, were nebulized into the aerosol VMI spectrometer for subsequent analysis. The N 1s level XPS spectra are presented in Fig. 5A, and the signal could be fitted by two partially-overlapping gaussian curves with maxima at 404.8 and 407.3 eV. To understand the nature of the N 1s peaks, we used DFT calculations and relevant literature on similar nitrogen-containing molecules. The bottom panel of Fig. 5A corresponds to a DFT calculation of the XPS spectrum for the free-base (Nic_{FB}) with a maximum at 403.1 eV, for a nicotine molecule protonated on the pyrrolidinic ring (Nic_{P}) with two maxima at 403.4 and 405.8 eV corresponding to an unprotonated pyridinic N atom and a protonated pyrrolidinic N atom, and for a 70%/30% combination of both. The DFT values are shifted by 1.8 eV on the absolute scale to overlap with the experimental results. The observed N 1s shift of ~2 eV upon nicotine protonation is qualitatively similar to our previous observations for arginine and histidine.[49, 50] For the neutral pyridinic system, albeit in the condensed organic crystal phase, there is a single peak that splits into two upon protonation and a binding energy shift upon protonation, to the blue of the neutral case. The fraction of neutral free-base nicotine, α_{FB}, was calculated by summing the corresponding areas of neutral and mono protonated fitted gaussian curves and free-base nicotine predominated over the protonated species, with α_{FB} = 0.72 to 0.80 across this wide pH range. This is very different from what is observed in solution at low pH (high acidity), where the dominant form should be diprotonated nicotine.

Analyses of the N K-edge NEXAFS spectra to describe the nicotine speciation at the core of the particles are presented in Fig. 5B. We used previous experimental and theoretical studies on organic crystals to decipher

the spectra and provide a qualitative analysis of the peak positions and shape. Ge et al.[51] using quantum mechanical/molecular mechanical methods on isonicotimide and comparing it to the results of Edwards et al.[52] showed that the X-ray absorption spectra was sensitive to proton transfer and the nature of hydrogen bonding. Guided by these studies, we interpret the strong peak shown in **Fig. 5B** for pH 10.4 at 399.0 eV emanating from the π_1* orbital of the pyridinyl nitrogen. In **Fig. 5B** for pH 2, two peaks of almost equal intensity show up at 399.0 eV and 401.0 eV, the second peak originating from a π_2* orbital, with an absolute value of 399.1 eV. Ge *et al*.[51] suggest the second peak has major contribution from a protonated nitrogen orbital, with an absolute value of 401.2 eV calculated by theory. In addition, the peak shape at the post-edge region between 400 – 415 eV shown in **Fig. 5B** is captured very well by the theoretical calculations of Ge et al. for both NEXAFS spectra at low and high pH. This analysis provides compelling evidence that the core of the aerosol does show more protonation as a function of pH compared to what was obtained by XPS from the surface described earlier, as can be seen in the change in peak heights of the π_1* and π_2* peaks located at 399.0 and 401.0 eV respectively. To quantify these results, we used literature spectra of pyridine and pyrrolidine molecules in the crystalline phase to generate a synthetic NEXAFS spectrum for free base nicotine and the spectrum of the structurally similar sarcosine to generate the protonated spectra. From this we obtained the fraction of neutral free-base, α_{FB} and compared to the particle surface results. The fraction of free-base in the core of the particles was lower and more sensitive to the solution pH, changing from α_{FB} = 0.34 in basic medium to α_{FB} = 0.05 at the most acidic tested condition in agreement with the analysis of the π* peak analysis described earlier. This study contributes to a growing body of evidence illustrating differential acid-base properties due to reduced hydration of ionic species at the surface of aerosol particles with respect to their core, and to bulk aqueous conditions.[53]

Future Directions

Deep eutectic solvents. Deep eutectic solvents (DES) are an important class of eutectics that are considered as alternatives to conventional organic solvents and ionic liquids in many applications owing to their versatile characteristics.[54] DESs consist of a hydrogen bond donor and an acceptor and to-date model studies have focused on mixtures of choline chloride (ChCl) and poly-alcohols.[55] At specific compositions, these form a eutectic mixture which resembles many characteristics of ionic liquids and organic solvents thanks to their complicated inter and intramolecular hydrogen-bond network.[56] Charge transfer and delocalization effects and the consequences on the hydrogen-bond network remain unresolved and controversial. Furthermore, hydration tends to make an already complex system even more difficult to

understand. Similar to the glycerol/water system, nano-structuring, and phase separations are also invoked in DESs.[56] Recent work on understanding the microstructure in DESs have successfully employed combinations of vibrational spectroscopies, X-ray scattering, and theoretical calculations to investigate DES mixtures at different compositions and DES-cosolvent mixtures.[57, 58] From our perspective, we will focus on coupling X-ray spectroscopy (especially NEXAFS) & scattering to vibrational spectroscopy to provide a unique view of the microstructure and dynamics in DES systems. We will start with the classic DES, glyceline (composed of ChCl and glycerol) phase system to understand how the changes in hydrogen-bond network lead to a eutectic mixture at specific concentrations. Beyond using THz time-domain spectroscopy and chip-based ATR-FTIR spectroscopy and X-ray spectroscopies, we propose to use Raman spectroscopy and X-ray scattering to shed new light into the underlying structure and dynamics. Probes which allow us to access low-frequency regions of the Raman spectrum up to 40 cm^{-1} will be coupled with photoelectron spectroscopy (PES). PES at the Cl $L_{2,3}$-, C K-, N K-, and O K-edges of glyceline will unravel the local electronic structure of the mixtures. Raman spectroscopy will be used to probe both the hydrogen-bond networks of the mixture using low-frequency modes, and probe intermolecular and intramolecular interactions in glyceline using the fingerprint and C-H and O-H stretching regions of the spectrum. Theory will play a crucial role in allowing us to decipher the electronic structure of these hydrogen bonded system and corresponding disruption of these bonds.

Hydrogen bonded organic frameworks. Connecting phase-change materials (PCMs) (vide infra) and DESs are hydrogen-bond networks and the changes impacted on them by including inorganic salts, which can be extended to build a new class of materials, hydrogen bonded organic frameworks (HOF). HOFs are porous solids that are self-assembled by organic molecules through hydrogen bond interactions.[59] Since hydrogen bonding is much weaker than the covalent and electrostatic bonds that drive the formation and stability of MOFs and covalent organic frameworks (COFs), the design rules for synthesizing these networks are still emerging and not clear at present.[60] However, the reversible nature and the weakness of the hydrogen bond, coupled with the ability to select the molecular backbone and hydrogen bonding moieties does allow synthesis in benign and green solvents (even water) and easy separation, purification and regeneration. Hence there has been an explosion of studies recently to try and understand the underlying kinetics and mechanisms of formation, and phase change dynamics that occur upon the input of external stimuli. However, fundamental understanding is still lacking at the molecular level and connecting structural details to the bulk crystal has proven elusive. We seek to understand hydrogen bonding in two systems which have garnered enormous interest recently in which we understand the X-ray spectroscopy of some of their constituent moieties. The first system is prepared from cationic tetra-amidinium or anionic tetra-sulfonates

components of Crystalline Porous Organic Salt-6 (CPO-6),[61, 62] while the second is based on the formation of a bicarbonate salt upon incorporation of CO_2 on to a glyoxal-bis(iminoguanidine) (GBIG) salt (**Fig. 6**).[63]

Beyond enormous potential for new materials for energy storage, transport, and carbon capture, the study of HOF dynamics may also answer fundamental and controversial questions on the nature of hydrogen bonding, such as the invocation of anti-electrostatic forces in their formation.[64] For instance, there is a lot of work being performed on phosphate-based systems to try and decipher what leads to anion-anion interactions and how hydrogen bonding can actually stabilize complexes and larger systems.[65] Evidence is garnered from X-ray crystallography in the solid state as to how hydroxy-anions dimerize and subsequently polymerize by overcoming long-range electrostatic repulsion. The short-range hydrogen bonds that form between the anionic donor and acceptor are what is termed an anti-electrostatic hydrogen bond. Indirect evidence for these kinds of bonding in phosphate systems in aqueous systems is provided by early work using Raman spectroscopy and more recent work from crystal structures derived from receptor stabilized anion-anion dimers, UV vis spectroscopy, isothermal calorimetry, and NMR spectroscopy.[65] However, an unequivocal observation of anti-electrostatic hydrogen bonding in phosphate solutions is lacking, and we hypothesize that X-ray spectroscopy coupled to vibrational spectroscopy could be a path forward. We have undertaken preliminary measurements of aqueous phosphoric acid solutions, and tracked changes in the XPS and NEXAFS spectra while varying concentrations and pH. The XPS data for 2M concentration at the O K- and P $L_{2,3}$-edges are shown in **Fig. 6C** and **6D** to demonstrate the feasibility of the approach. A determination of NEXAFS spectra particularly to understand ion partitioning between the core and surface of the aerosol, in conjunction with theory will be required to understand the nature of hydrogen bonding in these aerosols. Recently we used such an approach to study ammonium nitrate aerosols,[66] and while we used DFT to calculate the binding energies to decipher the XPS spectra, we did not have the tools to study NEXAFS theoretically. In that work we suggested that the nitrate anion has a slight propensity for the surface, while both ammonium and nitrate ions are present in equal measure in the bulk. In **Fig. 6A** and **6B**, we show the N K-edge & S $L_{2,3}$-edge NEXAFS spectra generated from an ammonium sulfate aerosol, a system of much interest in earth's atmosphere[67] and possibly also on other planets.[68] Superimposed on that figure are literature spectra for ammonium generated from a liquid jet[69] and theoretically calculated using time-dependent DFT calculations performed by Carter-Fenk and Head-Gordon.[70] These types of theoretical calculations using coupled clusters[71] and the more recent time-dependent DFT[70] provide profound insight into the nature of solvation and hydrogen bonding embedded in the NEXAFS spectra. In the case of the S $L_{2,3}$-edge NEXAFS, we could not find any literature theoretical results to compare to, however, our spectra fit reasonably well with the literature experimental data.[72] It is entirely possible that

the dynamics of hydrogen bonding are tied up with proton transfer in this highly protic system. Recent evidence for this is provided by coupling dielectric spectroscopy, quasi-elastic neutron and light scattering.[73] In this work, it was determined that protons move via short jumps (0.5 – 0.7 Å) and the Grotthuss mechanism of proton hopping was invoked. Molecular dynamics simulations provide insight into the hydrogen-bond network in aqueous phosphoric acid systems and directly implicate proton transfer as being responsible for the topology.[74] Graph theory showed that the phosphoric acid hydrogen-bond network is highly robust even up to 50% addition of water, however the reverse is true for water's network. Even a slight addition of phosphoric acid to water leads to a complete breakdown of water's hydrogen-bond network, and is effectively a structure breaker. We believe that X-ray and vibrational spectroscopy employed by us to decipher the hydrogen-bond network in glycerol-water systems will also provide critical insight into an understanding of the nature of hydrogen bonding in the phosphoric-acid water system.

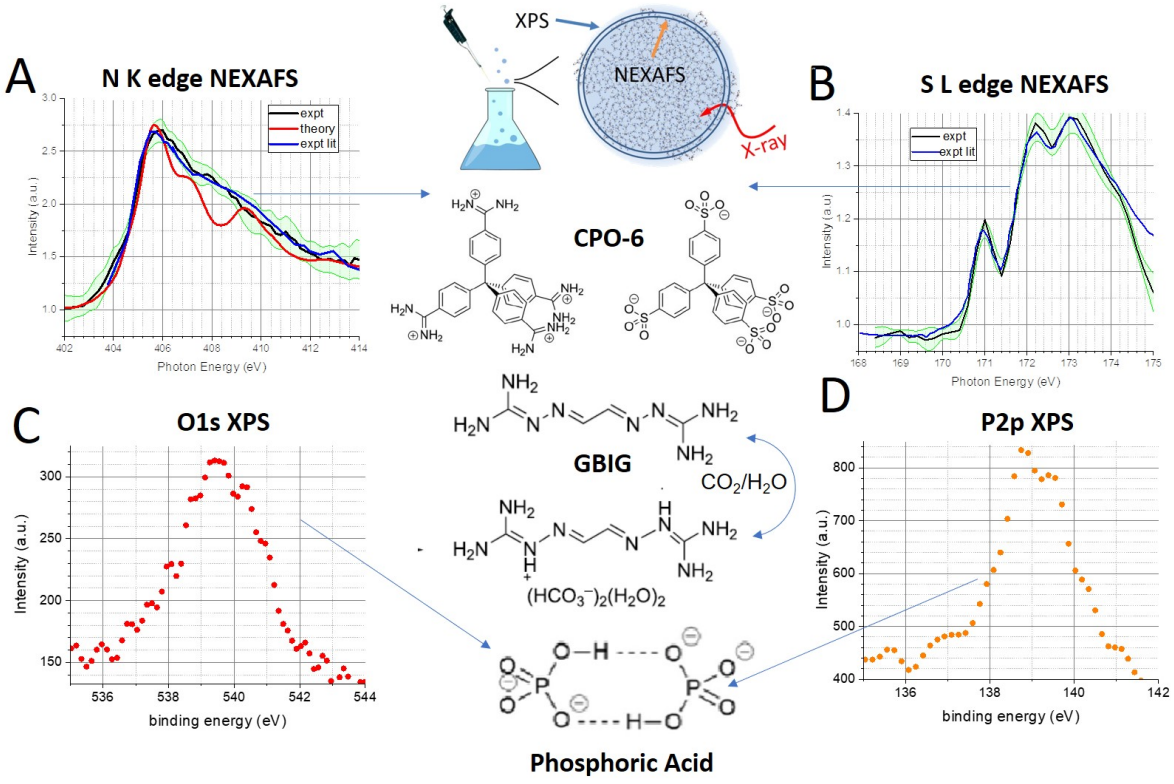

Figure 6. Schematic depicting ammonium sulfate aerosols with XPS and NEXAFS detecting surface and bulk respectively. (**A**) N L-edge NEXAFS spectra generated from an ammonium sulfate aerosol (in black with errors constrained in green). The red line is a theoretical calculation from Ref. 70 using TDDFT, and the blue line is the data from literature generated using liquid jets from Ref. 69. (**B**) S $L_{2,3}$-edge NEXAFS spectra generated from an ammonium sulfate aerosol (in black with errors constrained in green). The blue line is

data collected from sulfate aerosols deposited on a filter and measured using scanning transmission X-ray microscopy, from Ref. 72. Also shown in the figure are molecular structures for the CPO-6 precursors,[61, 62] the crystallization pathway for GBIG,[63] and the hydrogen bonding in a phosphoric acid dimer.

Finally, we introduce a new direction being undertaken at Berkeley Lab to couple soft X-ray scattering to directly probe free aerosols in vacuum. Many years ago, we successfully demonstrated this approach by using VUV light to probe Mie scattering on silica nanoparticles.[75] Scattering is a valuable method for providing information both on structural changes during phase transitions and on dimensions of crystallization nuclei at the relevant, nanometer length scale. Performed in resonance (with absorption edge) conditions using soft X-ray radiation, the technique allows for probing chemical composition of the system under study. There is an emerging body of work where X-ray scattering (SAXS/WAXS) using tender and hard X-rays to study structure particularly in levitated droplets relevant to aerosol chemistry.[76, 77] Herein, we describe how we have coupled an X-ray detector to our aerosol apparatus to simultaneously perform X-ray scattering with spectroscopy (**Fig. 1C**). We note a similar approach has been undertaken at the ALS for grazing incidence studies on surfaces.[78] Our technique allows for a complete multi-modal and in-situ way of probing aerosol chemistry and also processes such as crystallization and growth processes in HOFs and DES systems. We showcase a recent result using oleic acid as an example which acts as a surrogate for atmospheric aerosols, and as there is SAXS literature on the effects of humidity and ozonation on this particular molecule.[76, 77] Furthermore, we have knowledge of X-ray spectroscopy of similar organic aerosols[15, 79] coupled with an understanding of its vibrational and scattering properties based upon our own recent work on its self-assembly with arginine.[6] The formation and nucleation of particles from gas-phase precursors, physical and chemical processes on the particle surface and in the bulk span a range of temporal and spatial scales. These aerosols can exist in different phase states: solid, liquid, and highly viscous, which can change the atmospheric fate of these particles.[80] In viscous, diffusion-limited aerosols, species at the aerosol surface are expected to react more rapidly than molecules residing in the nanoparticle interior, forming steep chemical gradients. Surface-sensitive techniques, such as soft XPS, coupled with X-ray scattering will probe phase changes and structure simultaneously and will be of enormous benefit. **Fig. 7A** shows the C K-edge NEXAFS spectra from 1-µm-diameter oleic acid aerosol generated via a condensation monodisperse aerosol generator. At a chosen wavelength from this NEXAFS spectra, we perform X-ray scattering and an example is shown in **Fig. 7B** as the result. A section of the raw data is shown, and upon symmetrization to remove the shadow of the beam block, meaningful Q space results can be obtained. In the figure are shown the range of Q accessible and the C soft X-ray region. These images will change as

chemistry occurs on the aerosol and will allow us to capture diffusion dynamics and reaction kinetics under study within the timescale of the measurement (10 – 30s).

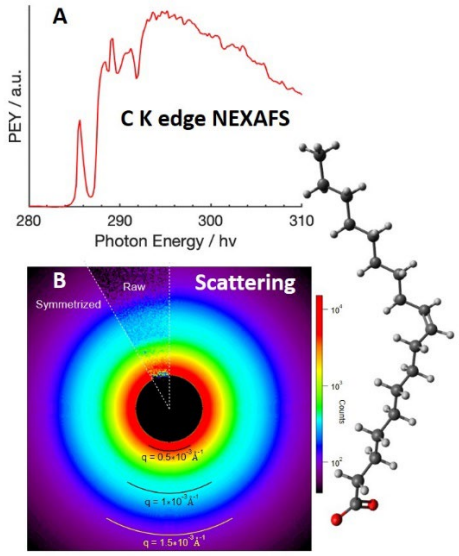

Figure 7. (A) C K-edge NEXAFS spectra, and (B) X-ray scattering from a 1 µm oleic acid aerosol. On the right is a schematic of the oleate anion.

Conclusion

As the world warms up, sequestering carbon dioxide, extracting water from ambient air, and storing energy in hydrogen bonds are some scientific directions that motivate us. To tackle the challenges of decarbonizing energy sources and mitigating climate change, we will need new infrastructure and ways of probing the complex chemical environments required for energy generation, storage and transport. In the last few years, we have learned to be nimble and deploy resources between table-top spectrometers and synchrotron from which the X-rays emanate. The Advanced Light Source (ALS) is over 30 years old, and will soon be replaced by a diffraction limited light source. In addition, Berkeley Lab is going through a renovation in space and infrastructure (indeed some buildings being replaced date from the Manhattan project in the 40's) and plans are afoot to build a Chemical Observatory. The vision is to have multiple experimental platforms within large, open laboratory spaces equipped with access ports to deliver X-rays from the revamped ALS coupled with traditional "lab" based tools such as lasers, electron & force microscopes, and nuclear magnetic resonance spectrometers. The initiative to upgrade the ALS to a diffraction-limited storage ring will provide full transverse coherence in its light output, perhaps as early as 2027. This will provide new capabilities that bridge local and global dynamics, connecting fundamental electronic, structural, and chemical dynamics with the collective phenomena of extended systems. Emerging

exceptionally powerful X-ray spectroscopy methods such as X-ray photon correlation spectroscopy, and resonant inelastic X-ray scattering with sub-natural line width will be enabled to probe hydrogen bonds. We have embarked on a path where we seek to adiabatically build upon what has been achieved so far and transition it towards this new way of doing science in the 21st energy. One can imagine a space where X-rays coupled to vibrational spectroscopies on the nanoscale will probe the molecular and structural dynamics of a hydrogen bonded organic framework which will one day be part of an energy storage framework/infrastructure that will make our world a cooler and sustainable place to live in.

Biography

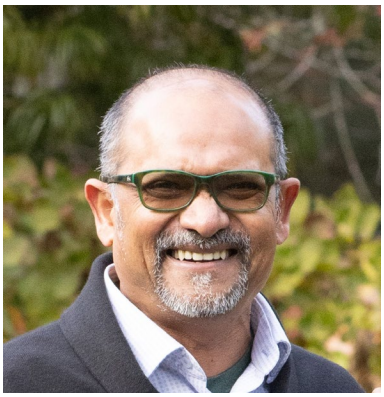

Musahid Ahmed is a senior scientist at Lawrence Berkeley National Labs, Berkeley, USA. He received his PhD in 1989 at Cambridge University and then went on to pursue postdoctoral fellowships at Leicester, Gottingen, and Manchester. He started probing water cluster beams with vacuum ultraviolet radiation at the Daresbury synchrotron which led him to join Berkeley lab in 1995 to pursue a career in using photon tools with molecular beams. Probing gas, interfacial and condensed phase chemical dynamics with X-ray, infrared and terahertz spectroscopy is his passion. Recently he has discovered that ultrafast spectroscopy, X-Ray scattering and Raman spectroscopy are cool tools to allow him to chip away at deciphering dynamics in complex systems.

Wenchao Lu received his Ph.D. from the City University of New York, New York, USA, in 2018. He then worked as a postdoctoral fellow at Lawrence Berkeley National Laboratory, Berkeley, USA, with Dr. Musahid Ahmed on probing gas- and condensed-phase molecular dynamics using spectroscopies. He is now a research scientist at Commonwealth Scientific and Industrial Research Organisation (CSIRO), Australia, where he focuses on evaluating the influence of per- and polyfluoroalkyl substances (PFAS) in the environment and seeking solutions to mitigate the impact.

Acknowledgments

The authors are indebted to all our co-workers at Berkeley Lab for the results presented here, particularly since the bulk of this work was performed under very trying circumstances during the COVID pandemic (Emily Zhang, Chaya Weeraratna, Chandika Amarasinghe, Nabiha Hasan, Ishan Gupta, Xena Quach, Amanda Sayaseng, Sorren Warkander, Pyeongeun Kim, Eleanor Greenspoon, Ryan Reynolds, Nureshan Dias, Alexander Lemmens). We also benefit enormously with collaborations with Kevin Wilson, Oleg Kostko, Jin Qian, Ayumi Koishi, Sumanjeet Kaur, Ravi Prasher, Andrew Martin, Zhi Huang, Anubhav Jain, Jeffery Long, Megan Jackson, Hugo Destaillats, Xiaochen Tang, Martin Head-Gordon, Kevin Carter-Fenk, Anna Krylov, Jennifer Bergner, Monika Blum, Ethan Crumlin, Chenhui Zhu, Slavomir Nemsak, Jian Zhang & Stephanie Gilbert-Corder. The authors gratefully acknowledge support from the Director, Office of Energy Research, Office of Basic Energy Sciences, Chemical Sciences Division of the U.S. Department of Energy under contract No. DE-AC02-05CH112311, through the Condensed Phase Interfaces and Molecular Sciences program. The ALS & NERSC is supported through the same contract. The work on protonation of nicotine in aqueous aerosols was partly supported by the University of California's Tobacco Related Diseases Research Program (TRDRP) project T31IP1722.

References

(1) Ahmed, M.; Blum, M.; Crumlin, E. J.; Geissler, P. L.; Head-Gordon, T.; Limmer, D. T.; Mandadapu, K. K.; Saykally, R. J.; Wilson, K. R. Molecular properties and chemical transformations near interfaces. *J. Phys. Chem. B* 2021, *125* (32), 9037-9051.

(2) Israelachvili, J. N. Part I: The forces between atoms and molecules. In *Intermolecular and Surface Forces (Third Edition)*, Israelachvili, J. N. Ed.; Academic Press, 2011; pp 3-22.

(3) Dill, K. A.; MacCallum, J. L. The protein-folding problem, 50 years on. *Science* 2012, *338* (6110), 1042-1046.

(4) Glotzer, S. C.; Solomon, M. J. Anisotropy of building blocks and their assembly into complex structures. *Nat. Mater.* 2007, *6* (8), 557-562.

(5) Zhang, J.; Li, S.; Le, W. Advances of terahertz technology in neuroscience: Current status and a future perspective. *iScience* 2021, *24* (12), 103548.

(6) Lu, W.; Zhang, E.; Amarasinghe, C.; Kostko, O.; Ahmed, M. Probing self-assembly in arginine-oleic acid solutions with terahertz spectroscopy and X-ray scattering. *J. Phys. Chem. Lett.* 2020, *11* (21), 9507-9514.

(7) Lu, W.; Amarasinghe, C.; Zhang, E.; Martin, A.; Kaur, S.; Prasher, R.; Ahmed, M. Probing hydrogen-bond networks in plastic crystals with terahertz and infrared spectroscopy. *Cell Rep. Phys. Sci.* 2022, *3* (8), 100988.

(8) Alexander, H.; Wim, B.; James, G.; Eric, S.; Eliot, G.; Rick, K.; Alastair, M.; Matthew, C.; Bruce, R.; Howard, P. A SAXS/WAXS/GISAXS beamline with multilayer monochromator. *J. Phys. Conf. Ser.* 2010, *247* (1), 012007.

(9) Sood, A.; Poletayev, A. D.; Cogswell, D. A.; Csernica, P. M.; Mefford, J. T.; Fraggedakis, D.; Toney, M. F.; Lindenberg, A. M.; Bazant, M. Z.; Chueh, W. C. Electrochemical ion insertion from the atomic to the device scale. *Nat. Rev. Mater.* 2021, *6* (9), 847-867.

(10) Wu, R.; Matta, M.; Paulsen, B. D.; Rivnay, J. Operando characterization of organic mixed ionic/electronic conducting materials. *Chem. Rev.* 2022, *122* (4), 4493-4551.

(11) Koishi, A.; Fernandez-Martinez, A.; Ruta, B.; Jimenez-Ruiz, M.; Poloni, R.; di Tommaso, D.; Zontone, F.; Waychunas, G. A.; Montes-Hernandez, G. Role of impurities in the kinetic persistence of amorphous calcium carbonate: a nanoscopic dynamics view. *J. Phys. Chem. C* 2018, *122* (29), 16983-16991.

(12) Reif, B.; Ashbrook, S. E.; Emsley, L.; Hong, M. Solid-state NMR spectroscopy. *Nat. Rev. Methods Primers* 2021, *1* (1), 2.

(13) Lilley, D.; Yu, P.; Ma, J.; Jain, A.; Prasher, R. Thermal fluids with high specific heat capacity through reversible Diels-Alder reactions. *iScience* 2022, *25* (1), 103540.

(14) Lu, W.; Zhang, E.; Qian, J.; Weeraratna, C.; Jackson, M. N.; Zhu, C.; Long, J. R.; Ahmed, M. Probing growth of metal-organic frameworks with X-ray scattering and vibrational spectroscopy. *Phys. Chem. Chem. Phys.* 2022, *24* (42), 26102-26110.

(15) Kostko, O.; Xu, B.; Jacobs, M. I.; Ahmed, M. Soft X-ray spectroscopy of nanoparticles by velocity map imaging. *J. Chem. Phys.* 2017, *147* (1), 013931.

(16) Mogaki, R.; Hashim, P. K.; Okuro, K.; Aida, T. Guanidinium-based "molecular glues" for modulation of biomolecular functions. *Chem. Soc. Rev.* 2017, *46* (21), 6480-6491.

(17) Li, B.; Kawakita, Y.; Ohira-Kawamura, S.; Sugahara, T.; Wang, H.; Wang, J.; Chen, Y.; Kawaguchi, S. I.; Kawaguchi, S.; Ohara, K.; et al. Colossal barocaloric effects in plastic crystals. *Nature* 2019, *567* (7749), 506-510.

(18) Huang, Z.; Kaur, S.; Ahmed, M.; Prasher, R. Water freezes at near-zero temperatures using carbon nanotube-based electrodes under static electric fields. *ACS Appl. Mater. Interfaces.* 2020, *12* (40), 45525-45532.

(19) Dalla Bernardina, S.; Paineau, E.; Brubach, J.-B.; Judeinstein, P.; Rouzière, S.; Launois, P.; Roy, P. Water in carbon nanotubes: The peculiar hydrogen bond network revealed by infrared spectroscopy. *J. Am. Chem. Soc.* 2016, *138* (33), 10437-10443.

(20) Wang, Y.; Jiang, L.; Shen, Q.; Shen, J.; Han, Y.; Zhang, H. Investigation on the self-assembled behaviors of C18 unsaturated fatty acids in arginine aqueous solution. *RSC Adv.* 2017, *7* (66), 41561-41572.

(21) Wang, Y.; Jiang, L.; Wei, C.; Zhang, H. Phase behaviors and self-assembled properties of ion-pairing amphiphile molecules formed by medium-chain fatty acids and L-arginine triggered by external conditions. *New J. Chem.* 2017, *41* (23), 14486-14497.

(22) Parrott, E. P. J.; Zeitler, J. A. Terahertz time-domain and low-frequency raman spectroscopy of organic materials. *Appl. Spectrosc.* 2015, *69* (1), 1-25.

(23) Steiner, T. The hydrogen bond in the solid state. *Angew. Chem. Int. Ed.* 2002, *41* (1), 48-76.

(24) Stevens, J. S.; Byard, S. J.; Seaton, C. C.; Sadiq, G.; Davey, R. J.; Schroeder, S. L. M. Proton transfer and hydrogen bonding in the organic solid state: a combined XRD/XPS/ssNMR study of 17 organic acid–base complexes. *Phys. Chem. Chem. Phys.* 2014, *16* (3), 1150-1160.
(25) Araujo, C. F.; Coutinho, J. A. P.; Nolasco, M. M.; Parker, S. F.; Ribeiro-Claro, P. J. A.; Rudić, S.; Soares, B. I. G.; Vaz, P. D. Inelastic neutron scattering study of reline: shedding light on the hydrogen bonding network of deep eutectic solvents. *Phys. Chem. Chem. Phys.* 2017, *19* (27), 17998-18009, 10.1039/C7CP01286A.
(26) Lloveras, P.; Aznar, A.; Barrio, M.; Negrier, P.; Popescu, C.; Planes, A.; Manosa, L.; Stern-Taulats, E.; Avramenko, A.; Mathur, N. D.; et al. Colossal barocaloric effects near room temperature in plastic crystals of neopentylglycol. *Nat. Commun.* 2019, *10* (1), 1803.
(27) Tran, K. T. T.; Le, L. T. M.; Phan, A. L. B.; Tran, P. H.; Vo, T. D.; Truong, T. T. T.; Nguyen, N. T. B.; Garg, A.; Le, P. M. L.; Tran, M. V. New deep eutectic solvents based on ethylene glycol - LiTFSI and their application as an electrolyte in electrochemical double layer capacitor (EDLC). *J. Mol. Liq.* 2020, *320*, 114495.
(28) Zhang, Z.; Liu, X.-Y. Control of ice nucleation: freezing and antifreeze strategies. *Chem. Soc. Rev.* 2018, *47*, 7116-7139.
(29) Sellberg, J. A.; Huang, C.; McQueen, T. A.; Loh, N. D.; Laksmono, H.; Schlesinger, D.; Sierra, R. G.; Nordlund, D.; Hampton, C. Y.; Starodub, D.; et al. Ultrafast X-ray probing of water structure below the homogeneous ice nucleation temperature. *Nature* 2014, *510*, 381.
(30) Ehre, D.; Lavert, E.; Lahav, M.; Lubomirsky, I. Water freezes differently on positively and negatively charged surfaces of pyroelectric materials. *Science* 2010, *327* (5966), 672-675.
(31) Morhart, T. A.; Read, S. T.; Wells, G.; Jacobs, M.; Rosendahl, S. M.; Achenbach, S.; Burgess, I. J. Micromachined multigroove silicon ATR FT-IR internal reflection elements for chemical imaging of microfluidic devices. *Anal. Methods* 2019, *11* (45), 5776-5783.
(32) Zhou, H.-C.; Long, J. R.; Yaghi, O. M. Introduction to metal–organic frameworks. *Chem. Rev.* 2012, *112* (2), 673-674.
(33) Desiraju, G. R. Crystal engineering: From molecule to crystal. *J. Am. Chem. Soc.* 2013, *135* (27), 9952-9967.
(34) Demir, H.; Daglar, H.; Gulbalkan, H. C.; Aksu, G. O.; Keskin, S. Recent advances in computational modeling of MOFs: From molecular simulations to machine learning. *Coord. Chem. Rev.* 2023, *484*, 215112.
(35) Gualtieri, A. F. Synthesis of sodium zeolites from a natural halloysite. *Phys. Chem. Miner.* 2001, *28* (10), 719-728.
(36) El Osta, R.; Feyand, M.; Stock, N.; Millange, F.; Walton, R. I. Crystallisation kinetics of metal organic frameworks from in situ time-resolved X-ray diffraction. *Powder Diffr.* 2013, *28* (S2), S256-S275.
(37) Strauss, I.; Mundstock, A.; Treger, M.; Lange, K.; Hwang, S.; Chmelik, C.; Rusch, P.; Bigall, N. C.; Pichler, T.; Shiozawa, H.; et al. Metal–organic framework Co-MOF-74-based host–guest composites for resistive gas sensing. *ACS Appl. Mater. Interfaces.* 2019, *11* (15), 14175-14181.
(38) Shi, F.; Wang, Z.; Zhu, K.; Zhu, X.; Yang, W. Enhancing activity and stability of Co-MOF-74 for oxygen evolution reaction by wrapping polydopamine. *Electrochim. Acta* 2022, *416*, 140293.
(39) Ewing, G. E.; Foster, M.; Cantrell, W.; Sadtchenko, V. Thin film water on insulator surfaces. In *Water in Confining Geometries*, Buch, V., Devlin, J. P. Eds.; Springer Berlin Heidelberg, 2003; pp 179-211.
(40) Wang, H.; Park, M.; Dong, R.; Kim, J.; Cho, Y.-K.; Tlusty, T.; Granick, S. Boosted molecular mobility during common chemical reactions. *Science* 2020, *369* (6503), 537-541.
(41) Rovelli, G.; Jacobs, M. I.; Willis, M. D.; Rapf, R. J.; Prophet, A. M.; Wilson, K. R. A critical analysis of electrospray techniques for the determination of accelerated rates and mechanisms of chemical reactions in droplets. *Chem. Sci.* 2020, *11* (48), 13026-13043.
(42) Oh, K.-I.; Baiz, C. R. Molecular heterogeneity in aqueous cosolvent systems. *J. Chem. Phys.* 2020, *152* (19), 190901.
(43) Ahmed, M.; Kostko, O. From atoms to aerosols: probing clusters and nanoparticles with synchrotron based mass spectrometry and X-ray spectroscopy. *Phys. Chem. Chem. Phys.* 2020, *22* (5), 2713-2737.
(44) Pellegrin, E.; Perez-Dieste, V.; Escudero, C.; Rejmak, P.; Gonzalez, N.; Fontsere, A.; Prat, J.; Fraxedas, J.; Ferrer, S. Water/methanol solutions characterized by liquid μ-jet XPS and DFT—The methanol hydration case. *J. Mol. Liq.* 2020, *300*, 112258.
(45) Dey, S.; Folkestad, S.; Paul, A.; Koch, H.; Krylov, A. Core-ionization spectrum of liquid water. *ChemRxiv* 2023.
(46) Weeraratna, C.; Amarasinghe, C.; Lu, W.; Ahmed, M. A direct probe of the hydrogen bond network in aqueous glycerol aerosols. *J. Phys. Chem. Lett.* 2021, *12* (23), 5503-5511.

(47) Charkhesht, A.; Lou, D.; Sindle, B.; Wen, C.; Cheng, S.; Vinh, N. Q. Insights into hydration dynamics and cooperative interactions in glycerol-water mixtures by terahertz dielectric spectroscopy. *J. Phys. Chem. B* **2019**, *123* (41), 8791-8799.
(48) Weeraratna, C.; Tang, X.; Kostko, O.; Rapp, V. H.; Gundel, L. A.; Destaillats, H.; Ahmed, M. Fraction of free-base nicotine in simulated vaping aerosol particles determined by X-ray spectroscopies. *J. Phys. Chem. Lett.* **2023**, *14* (5), 1279-1287.
(49) Kostko, O.; Xu, B.; Ahmed, M. Local electronic structure of histidine in aqueous solution *Phys. Chem. Chem. Phys.* **2021**, *23* (14), 8847-8853.
(50) Xu, B.; Jacobs, M. I.; Kostko, O.; Ahmed, M. Guanidinium group remains protonated in a strongly basic arginine solution. *ChemPhysChem* **2017**, *18* (12), 1503-1506.
(51) Ge, G.; Zhang, J.-R.; Wang, S.-Y.; Wei, M.; Hua, W. A QM/MM study on the X-Ray spectra of organic proton transfer crystals of isonicotinamides. *J. Phys. Chem. C* **2022**, *126*, 15849-15863.
(52) Edwards, P. T.; Saunders, L. K.; Grinter, D. C.; Ferrer, P.; Held, G.; Shotton, E. J.; Schroeder, S. L. M. Determination of H-atom positions in organic crystal structures by NEXAFS combined with density functional theory: A study of two-component systems containing isonicotinamide. *J. Phys. Chem. A* **2022**, *126*, 2889-2898.
(53) Colussi, A. J.; Enami, S.; Ishizuka, S. Hydronium ion acidity above and below the interface of aqueous microdroplets. *ACS Earth Space Chem.* **2021**, *5*, 2341-2346.
(54) Liu, Y.; Friesen, J. B.; McAlpine, J. B.; Lankin, D. C.; Chen, S. N.; Pauli, G. F. Natural deep eutectic solvents: Properties, applications, and perspectives. *J. Nat. Prod.* **2018**, *81* (3), 679-690.
(55) Wang, H.; Liu, S.; Zhao, Y.; Wang, J.; Yu, Z. Insights into the hydrogen bond interactions in deep eutectic solvents composed of choline chloride and polyols. *ACS Sustain. Chem. Eng.* **2019**, *7* (8), 7760-7767.
(56) Kaur, S.; Kumari, M.; Kashyap, H. K. Microstructure of deep eutectic solvents: Current understanding and challenges. *J. Phys. Chem. B* **2020**, *124* (47), 10601-10616.
(57) Schaeffer, N.; Abranches, D. O.; Silva, L. P.; Martins, M. A. R.; Carvalho, P. J.; Russina, O.; Triolo, A.; Paccou, L.; Guinet, Y.; Hedoux, A.; et al. Non-ideality in thymol + menthol type V deep eutectic solvents. *ACS Sustain. Chem. Eng.* **2021**, *9* (5), 2203-2211.
(58) Mannucci, G.; Busato, M.; Tofoni, A.; D'Angelo, P. Structural evolution of the butylated hydroxytoluene/menthol hydrophobic eutectic solvent upon methanol and ethanol cosolvent addition. *J. Mol. Liq.* **2023**, *375*, 121302.
(59) Lin, R.-B.; Chen, B. Hydrogen-bonded organic frameworks: Chemistry and functions. *Chem* **2022**, *8* (8), 2114-2135.
(60) Song, X.; Wang, Y.; Wang, C.; Wang, D.; Zhuang, G.; Kirlikovali, K. O.; Li, P.; Farha, O. K. Design rules of hydrogen-bonded organic frameworks with high chemical and thermal stabilities. *J. Am. Chem. Soc.* **2022**, *144* (24), 10663-10687.
(61) Zhang, S.; Fu, J.; Das, S.; Ye, K.; Zhu, W.; Ben, T. Crystalline porous organic salt for ultrarapid adsorption/desorption-based atmospheric water harvesting by dual hydrogen bond system. *Angew. Chem. Int. Ed.* **2022**, *61* (40), e202208660.
(62) Muang-Non, P.; Richardson, C.; White, N. G. Correspondence on "Crystalline porous organic salt for ultrarapid adsorption/desorption-based atmospheric water harvesting by dual hydrogen bond system". *Angew. Chem. Int. Ed.* **2023**, *62* (8), e202212962.
(63) Williams, N. J.; Seipp, C. A.; Brethomé, F. M.; Ma, Y.-Z.; Ivanov, A. S.; Bryantsev, V. S.; Kidder, M. K.; Martin, H. J.; Holguin, E.; Garrabrant, K. A.; et al. CO_2 capture via crystalline hydrogen-bonded bicarbonate dimers. *Chem* **2019**, *5* (3), 719-730.
(64) Weinhold, F.; Klein, R. A. Anti-electrostatic hydrogen bonds. *Angew. Chem. Int. Ed.* **2014**, *53*, 11214-11217.
(65) Zhao, W.; Flood, A. H.; White, N. G. Recognition and applications of anion-anion dimers based on anti-electrostatic hydrogen bonds (AEHBs). *Chem. Soc. Rev.* **2020**, *49* (22), 7893-7906.
(66) Weeraratna, C.; Kostko, O.; Ahmed, M. An investigation of aqueous ammonium nitrate aerosols with soft X-ray spectroscopy. *Mol. Phys.* **2022**, *120* (1-2), e1983058.
(67) Kong, X.; Castarede, D.; Thomson, E. S.; Boucly, A.; Artiglia, L.; Ammann, M.; Gladich, I.; Pettersson, J. B. C. A surface-promoted redox reaction occurs spontaneously on solvating inorganic aerosol surfaces. *Science* **2021**, *374* (6568), 747-752.
(68) Fauré, N.; Chen, J.; Artiglia, L.; Ammann, M.; Bartels-Rausch, T.; Li, J.; Liu, W.; Wang, S.; Kanji, Z. A.; Pettersson, J. B. C.; et al. Unexpected behavior of chloride and sulfate ions upon surface solvation of Martian salt analogue. *ACS Earth Space Chem.* **2023**, *7* (2), 350-359.

(69) Ekimova, M.; Quevedo, W.; Szyc, L.; Iannuzzi, M.; Wernet, P.; Odelius, M.; Nibbering, E. T. J. Aqueous solvation of ammonia and ammonium: probing hydrogen bond motifs with FT-IR and soft X-ray spectroscopy. *J. Am. Chem. Soc.* 2017, *139* (36), 12773-12783.
(70) Carter-Fenk, K.; Head-Gordon, M. On the choice of reference orbitals for linear-response calculations of solution-phase K-edge X-ray absorption spectra. *Phys. Chem. Chem. Phys.* 2022, *24* (42), 26170-26179.
(71) Reinholdt, P.; Vidal, M. L.; Kongsted, J.; Iannuzzi, M.; Coriani, S.; Odelius, M. Nitrogen K-edge X-ray absorption spectra of ammonium and ammonia in water solution: assessing the performance of polarizable embedding coupled cluster methods. *J. Phys. Chem. Lett.* 2021, *12* (36), 8865-8871.
(72) Hopkins, R. J.; Desyaterik, Y.; Tivanski, A. V.; Zaveri, R. A.; Berkowitz, C. M.; Tyliszczak, T.; Gilles, M. K.; Laskin, A. Chemical speciation of sulfur in marine cloud droplets and particles: Analysis of individual particles from the marine boundary layer over the California current. *J. Geophys. Res.* 2008, *113* (D4), D04209.
(73) Popov, I.; Zhu, Z.; Young-Gonzales, A. R.; Sacci, R. L.; Mamontov, E.; Gainaru, C.; Paddison, S. J.; Sokolov, A. P. Search for a Grotthuss mechanism through the observation of proton transfer. *Commun. Chem.* 2023, *6* (1), 77.
(74) Mikalciute, A.; Vilciauskas, L. Insights into the hydrogen bond network topology of phosphoric acid and water systems. *Phys. Chem. Chem. Phys.* 2021, *23* (10), 6213-6224.
(75) Shu, J.; Wilson, K. R.; Arrowsmith, A. N.; Ahmed, M.; Leone, S. R. Light scattering of ultrafine silica particles by VUV synchrotron radiation. *Nano Lett.* 2005, *5* (6), 1009-1015.
(76) Pfrang, C.; Rastogi, K.; Cabrera-Martinez, E. R.; Seddon, A. M.; Dicko, C.; Labrador, A.; Plivelic, T. S.; Cowieson, N.; Squires, A. M. Complex three-dimensional self-assembly in proxies for atmospheric aerosols. *Nat. Commun.* 2017, *8* (1), 1724.
(77) Milsom, A.; Squires, A. M.; Quant, I.; Terrill, N. J.; Huband, S.; Woden, B.; Cabrera-Martinez, E. R.; Pfrang, C. Exploring the nanostructures accessible to an organic surfactant atmospheric aerosol proxy. *J. Phys. Chem. A* 2022, *126* (40), 7331-7341.
(78) Kersell, H.; Chen, P.; Martins, H.; Lu, Q.; Brausse, F.; Liu, B. H.; Blum, M.; Roy, S.; Rude, B.; Kilcoyne, A.; et al. Simultaneous ambient pressure X-ray photoelectron spectroscopy and grazing incidence X-ray scattering in gas environments. *Rev. Sci. Instrum.* 2021, *92* (4), 044102.
(79) Jacobs, M. I.; Xu, B.; Kostko, O.; Wiegel, A. A.; Houle, F. A.; Ahmed, M.; Wilson, K. R. Using nanoparticle X-ray spectroscopy to probe the formation of reactive chemical gradients in diffusion-limited aerosols. *J. Phys. Chem. A* 2019, *123* (28), 6034-6044.
(80) Reid, J. P.; Bertram, A. K.; Topping, D. O.; Laskin, A.; Martin, S. T.; Petters, M. D.; Pope, F. D.; Rovelli, G. The viscosity of atmospherically relevant organic particles. *Nat. Commun.* 2018, *9* (1), 956.